

# Coupling of $\alpha$ -channeling to $|k_{\parallel}|$ upshift in lower hybrid current drive

I. E. Ochs,<sup>1</sup> N. Bertelli,<sup>2</sup> and N. J. Fisch<sup>3,2</sup>

<sup>1</sup>*Department of Physics, Harvard University, Cambridge, Massachusetts 02138*

<sup>2</sup>*Princeton Plasma Physics Laboratory, Princeton, New Jersey 08543*

<sup>3</sup>*Department of Astrophysical Sciences, Princeton University, Princeton, New Jersey 08540*

(Dated: August 27, 2022)

Although lower hybrid waves have been shown to be effective in driving plasma current in present-day tokamaks, they are predicted to strongly interact with the energetic  $\alpha$  particles born from fusion reactions in eventual tokamak reactors. In the presence of the expected strong  $\alpha$  particle birth gradient, however, this interaction can produce wave amplification rather than wave damping, but only if the launch position and orientation of the waveguides are suitably arranged. The flexibilities in achieving the amplification effect are identified through a consideration of symmetries in the channeling effect, in the wave propagation, and in the tokamak field configuration. Interestingly, for current drive that supports the poloidal magnetic field, the achievement of wave amplification through  $\alpha$  channeling is fundamentally coupled to effects leading to the elusive  $|k_{\parallel}|$  upshift.

PACS numbers: 52.35.-g, 52.55.Fa, 52.55.Wq, 52.55.-s

*Introduction:* Lower hybrid (LH) waves are predicted to be effective in driving substantial plasma current in tokamaks [1], an effect that has enjoyed extensive demonstration in tokamak experiments [2]. Yet there remains a concern that, in extrapolating to a fusion reactor, high-energy  $\alpha$  particles born in the plasma core could strongly damp the LH wave [3–5]. However, by coupling diffusion in energy to diffusion in space (known as *alpha channeling*), a favorable population inversion may appear along the diffusion path, causing the  $\alpha$  particles to amplify rather than damp the wave [6].

Recently, launching the LH wave from the tokamak high-field side (inside launch) was proposed to enable the LH wave to more deeply penetrate the plasma core, with the waveguide better protected from the plasma [7, 8]. Since in a reactor,  $\alpha$  particles would be abundant close to the plasma center, the question arises whether interactions of deeply penetrating waves with  $\alpha$  particles can be made favorable, while preserving high current drive efficiency. Despite many ray-tracing studies of LH waves to optimize the current drive effect [9–21], no study has optimized jointly for LH current drive and  $\alpha$ -channeling.

It turns out, in fact, that symmetries in the LH dispersion relation constrain the possibilities in simultaneously achieving current drive and  $\alpha$ -channeling. The channeling effect depends on the sign of poloidal wavenumber  $k_{\theta}$  [6], a dependency exploited in ion Bernstein waves [22], where particularly large wavenumbers could be arranged as a result of mode conversion [23]. For the LH wave,  $k_{\theta}$  similarly determines the channeling condition. However, it is the LH toroidal wavenumber  $k_{\phi}$  that determines the current drive direction through the wave interaction with electrons. For the LH wave,  $k_{\theta}$  is a function both of the launch geometry and the position along the ray [24]. Thus the joint optimization of the current drive and  $\alpha$ -channeling effects is fundamentally linked to the propagation of the wave.

We find that optimization is further constrained by an inescapable coupling of  $\alpha$ -channeling to the so-called “ $|k_{\parallel}|$  upshift”, where  $k_{\parallel}$  is the wavenumber parallel to the magnetic field. This upshift is thought to resolve the so-called “spectral gap” puzzle in LH wave interactions [25]. Since the phase velocity of injected waves appears to be too high to interact with electrons, only an upshift in  $|k_{\parallel}|$  along the ray will produce a resonance. The upshift itself, while well documented experimentally [26–28], continues to elude definitive explanation. The coupling constrains the flexibilities in achieving the  $\alpha$ -channeling effect.

By first considering a tokamak geometry with circular and concentric flux surfaces, we derive fundamental symmetries that constrain the joint optimization of current drive and  $\alpha$ -channeling. Interestingly, we find that an upshift must occur for LH waves that both support the channeling effect and drive current supportive of the poloidal magnetic field. Then, in a more realistic magnetic topology, we simulate how inside launch, with wave parameters chosen to localize the wave to where the  $\alpha$  particles have a steep gradient, jointly optimizes the channeling and current drive effects.

*Fundamental Constraints:* To see how channeling is constrained under LH wave propagation, consider that  $\alpha$  particles that gain energy from the interaction move in the direction of  $\mathbf{k} \times \mathbf{B}$ , while those that lose energy move in the direction of  $-\mathbf{k} \times \mathbf{B}$  (Fig. 1a). For “proper”  $\alpha$  channeling, the  $\alpha$  particles that gain energy move to the plasma center. Consider a tokamak with concentric, circular magnetic surfaces, so that the flux surface normal vector is given by  $\hat{\mathbf{r}}$ , the minor radius vector. Of interest then is the sign and magnitude of  $\xi \equiv \frac{\mathbf{k} \times \mathbf{B}}{|\mathbf{k} \times \mathbf{B}|} \cdot \hat{\mathbf{r}}$ . The magnitude of  $\xi$  represents the extent of the push in the radial direction, while the sign represents the direction of channeling: when  $\xi$  is negative, particles that gain energy will be pushed to the plasma center. Thus,  $\xi$  must be negative to reduce or reverse the damping. Since

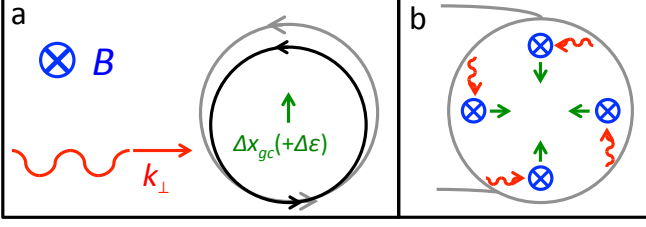


FIG. 1: (a) Schematic of the channeling effect, showing the coupling between  $\Delta x$  and  $\Delta \epsilon$ . When wave energy is channeled into the particles, they move in the direction of  $\mathbf{k} \times \mathbf{B}$ . (b) In a tokamak magnetic field configuration,  $\mathbf{B}$  (blue) is approximately aligned with the toroidal tangent vector  $\hat{\phi}$ , and so an inward-pointing  $\mathbf{k} \times \mathbf{B}$  (green) requires positive  $k_\theta$  (red). In this case,  $\xi \approx -k_\theta/k_\perp$ . Color available online.

$|B_\phi| \gg |B_\theta|$  and  $k_\perp \gg k_\parallel$ , it follows that

$$\xi \equiv \frac{\mathbf{k} \times \mathbf{B}}{|\mathbf{k} \times \mathbf{B}|} \cdot \hat{\mathbf{r}} \approx -\frac{k_\theta}{|k_\perp|} \quad (1)$$

where  $|k_\perp| = \sqrt{k_\theta^2 + k_r^2}$ . Thus, for  $B_\phi > 0$ , proper channeling requires  $k_\theta$  to be positive (Figure 1b).

For the LH wave, the sign of  $k_\theta$  turns out to be intimately connected with the poloidal launch angle: specifically,  $k_\theta$  tends to decrease along the ray above the poloidal equator ( $0^\circ < \theta < 180^\circ$ ), and increase below it. This effect is *independent of both the direction of current drive and the direction of the magnetic field*. To see this, consider a simple, well-known electrostatic model of dispersion for  $\Omega_i \ll \omega \ll \Omega_e$  in a tokamak of major radius  $R_0$  [24]:

$$D_0 \approx (c^2/\omega^2) \left( k_\perp^2 - (\omega_{pe}/\omega)^2 k_\parallel^2 \right) \quad (2)$$

$$B_\phi = B_{\phi 0}/[1 + (r/R_0) \cos \theta]. \quad (3)$$

Although this model is strictly valid only near  $k_\theta = 0$ , simulations show that the symmetries uncovered here also hold for the full dispersion relation. For tokamaks,  $B_\phi \gg B_\theta$  and  $\omega_{pe} \gg \omega$ , so that the initial evolution of  $k_\theta$  (when  $k_\theta \simeq 0$ ) is determined by

$$\begin{aligned} \frac{dk_\theta}{dt} &= \frac{\partial D_0/\partial \theta}{\partial D_0/\partial \omega} \\ &\approx - \left( \frac{B_\theta^2}{B_{\phi 0}^2} \right) \left( \frac{\omega^3 (R_0 + r \cos \theta)}{2\omega_{pe}^2 R_0^2} \right) \sin \theta, \end{aligned} \quad (4)$$

and

$$\frac{d\theta}{dt} = -\frac{\partial D_0/\partial m}{\partial D_0/\partial \omega} \approx \left( \frac{B_\theta}{B_{\phi 0} k_\phi} \right) \left( \frac{\omega (R_0 + r \cos \theta)}{2r R_0} \right). \quad (5)$$

For current drive supporting the poloidal magnetic field ( $k_\phi B_\theta > 0$ ), and for proper channeling ( $k_\theta B_\phi > 0$ ), it follows that  $B_\phi > 0$  requires  $dk_\theta/dt > 0$ . Since  $dk_\theta/dt \propto -\sin \theta$ ,  $k_\theta$  will increase along the ray when  $180^\circ < \theta < 360^\circ$ , and thus the final approach to the region of high  $\alpha$  particle density must occur *below the poloidal equator* to ensure proper channeling in a circular tokamak.

Several symmetries of the channeling effect, derived from Eqs. (4) and (5), are confirmed by the full geometrical optics ray equations (Fig. 2). First, for current drive supportive of the poloidal magnetic field ( $k_\phi B_\theta > 0$ ), the sign of  $B_\theta$  turns out to have no impact on the poloidal trajectory or the evolution of  $k_\theta$ . This follows directly from the fact that Eqs. (4) and (5) depend only on  $B_\theta^2$  and  $B_\theta/k_\phi$ . Thus  $\alpha$ -channeling is unaffected under coupled reversal of  $k_\phi$  and  $B_\theta$ . Second, under  $B_\phi$  reversal, proper channeling requires  $k_\theta$  reversal as well. Since Eq. (4) depends only on  $B_{\phi 0}^2$ , it follows that  $\sin \theta > 0$ , corresponding to launch from above the poloidal equator. Interestingly, this sign reversal in  $dk_\theta/dt$  ensures that, all other quantities equal, a launch with  $(k_\theta, \theta)$  when  $B_\phi > 0$  will have a perfectly antisymmetric poloidal trajectory and  $k_\theta$  evolution to the launch with  $(-k_\theta, -\theta)$  when  $B_\phi < 0$ , since Eq. (5) also changes sign with  $B_\phi$  (Figs. 2a and 2b).

Consider now that the  $|k_\parallel|$  shift is determined by the magnitude and sign of  $(k_\theta \cdot B_\theta)(k_\phi \cdot B_\phi) = (k_\theta B_\phi)(k_\phi B_\theta)$ . Since for supportive current drive  $k_\phi B_\theta > 0$ , and for proper channeling  $k_\theta B_\phi > 0$ , launching to ensure proper channeling gives  $|k_\parallel| > 0$  in the region of strong channeling regardless of the magnetic field geometry (Fig. 2d).

These constraints apply only for supportive current drive. However, for current drive that opposes  $B_\theta$  ( $k_\phi B_\theta < 0$ ), for example for current profile control, Eqs. (4) and (5) then show that although the sign of  $dk_\theta/dt$  stays the same, the sign of  $d\theta/dt$  is reversed, breaking the anti-symmetric evolution observed under

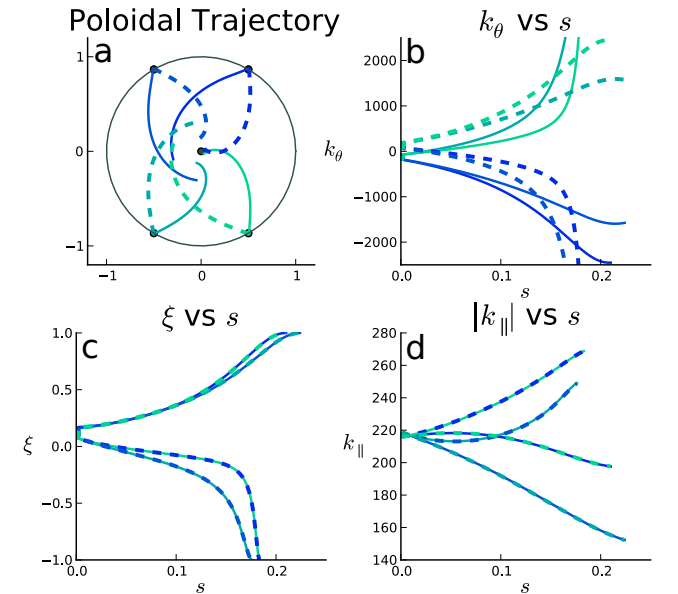


FIG. 2: Ray propagation symmetries with respect to  $B_\phi$  reversal in circular tokamak with 5 keV plasma. Solid lines:  $B_\phi > 0, k_\theta > 0$ ; dashed lines:  $B_\phi < 0, k_\theta < 0$ . Reversing  $B_\phi$ ,  $k_\theta$ , and  $\theta$  results in antisymmetric evolution in  $\theta$  and  $k_\theta$  (a-b). The reversals have no effect on  $\xi$  or the  $|k_\parallel|$  upshift however, which are clearly coupled (c-d). Color available online.

$B_\phi$  reversal. Interestingly, the trajectory resulting from reversed current drive for proper channeling is symmetric with respect to the trajectory resulting from supportive current drive for improper channeling ( $k_\theta B_\phi < 0$ ). Also, since  $k_\phi$  reverses sign while all other quantities remain the same, reversed current drive results inevitably in a  $|k_\parallel|$  downshift in the region of strong channeling.

These constraints and their associated symmetries, imposed through the fundamental coupling of  $\alpha$  channeling to LH current drive to the  $|k_\parallel|$ -upshift, are the key results here. Although derived strictly for concentric circular flux surfaces, they are valid in a more general magnetic geometry in the regime of interest, namely where the LH waves penetrate deeply enough to encounter  $\alpha$  particles at the locally circular plasma center. As an example, we now consider optimization in a reactor-like configuration.

*Required  $\alpha$ -particle birth gradient:* The alpha channeling effect results in diffusion paths in  $r - \epsilon_\perp$  space (where  $\epsilon_\perp = (v_\perp/v_\alpha)^2$  is normalized to the  $\alpha$ -particle birth energy  $\epsilon_\alpha$ ) obeying,

$$\frac{\partial \epsilon_\perp}{\partial r} = \frac{\Delta \epsilon_\perp}{\xi \Delta x_{gc}} = \frac{m_\alpha \Omega_\alpha \omega}{\xi k_\perp \epsilon_\alpha} = \frac{2Z_\alpha e B \omega}{\xi k_\perp m_\alpha v_\alpha^2}. \quad (6)$$

For an  $\alpha$ -particle distribution monotonically decreasing in energy on each flux surface, a steep radial gradient is required for wave amplification, as  $\alpha$  particles are diffused from high energy near the plasma center to low energy at the plasma periphery. The diffusion coefficient is

$$D(\epsilon_\perp) = \frac{2\omega}{\epsilon_w^3 (\epsilon_\perp - \epsilon_w)^{1/2}} \left( \frac{v_{osc}}{v_\alpha} \right)^2 H(\epsilon_\perp - \epsilon_w),$$

where  $\epsilon_w = (\omega/k_\perp)^2/v_\alpha^2$ ,  $v_{osc} = 2eE/m\omega$ , and  $H(x)$  is the Heaviside function [6].

For birth of energetic  $\alpha$  particles from fusion at rate  $\dot{N}_\alpha$ , the distribution of energetic  $\alpha$  particles, dominated by slowing down on electrons, is  $f(\epsilon_\perp, r) = \dot{N}_\alpha(r)/2\nu\epsilon_\perp$ , where  $\nu = 16\sqrt{2\pi m_e} e^4 n_e \times \ln \Lambda / 3T_e^{3/2} m_\alpha$ . Here we assume that the LH wave intensities are insufficient to modify the  $\alpha$ -particle distribution. For power in the wave given by  $P = v_g \epsilon_0 E^2 A/2$ , where  $A$  is the ray's cross-sectional area and  $v_g$  is the group velocity, the change in power along the ray length  $l$  is then given by

$$\frac{dP}{dl} = P \left( \frac{4Z_\alpha^2 e^2 \dot{N}_\alpha}{\nu \epsilon_0 m \omega \epsilon_w^3 v_g} \right) \times \left[ - \left( \frac{\sqrt{\epsilon_w - \epsilon_w^2} + \arccos \sqrt{\epsilon_w}}{\epsilon_w^{3/2}} \right) + \left( 2\xi \frac{\partial r}{\partial \epsilon_\perp} \right) \left( \frac{2 \arccos \sqrt{\epsilon_w}}{\epsilon_w^{1/2}} \right) \left( \frac{1}{f} \frac{\partial f}{\partial r} \right) \right]. \quad (7)$$

Substituting Eq. (6) into Eq. (7), and using  $\partial f / \partial r \approx d\dot{N}_\alpha / dr$ , gives the expression for the required (negative) radial decay length  $\lambda_0 \equiv \dot{N}_\alpha / (d\dot{N}_\alpha / dr)$  for zero damping:

$$\lambda_0^{-1} = \frac{1 + \sqrt{\epsilon_w - \epsilon_w^2} / \arccos \sqrt{\epsilon_w}}{4} \left( \frac{2Z_\alpha e}{m_\alpha \omega} \right) \left( \frac{k_\perp B}{\xi} \right). \quad (8)$$

When  $\frac{1}{\dot{N}_\alpha} \frac{d\dot{N}_\alpha}{dr}$  is negative and  $\left| \frac{1}{\dot{N}_\alpha} \frac{d\dot{N}_\alpha}{dr} \right| > |\lambda_0^{-1}|$ , the  $\alpha$  particles will amplify, rather than damp, the wave.

*Example of Joint Optimization:* As an example of joint optimization of the current-drive and  $\alpha$ -channeling effects in the reactor regime, consider a nearly circular equilibrium [29], with parameters suggested by the ARC tokamak reactor [8]. Accordingly, take major radius  $R = 3.45\text{m}$  and minor radius  $a = 1.13\text{m}$ . The current is 7.8 MA and the toroidal magnetic field is 9.25 T. The safety factor  $q$  is monotonically increasing from the magnetic axis, with  $q(\text{axis}) = 1.015$  and  $q(\text{edge}) = 2.693$ . The temperature and density profiles for electrons and ions are given analytically on each flux surface by

$$T(r) = (T_{\max} - T_{\min}) (1 - r^2/a^2)^2 + T_{\min}$$

$$n(r) = (n_{\max} - n_{\min}) (1 - r^2/a^2)^2 + n_{\min}$$

where  $T_{\max} = 5 \text{ keV}$ ,  $T_{\min} = 500 \text{ eV}$ ,  $n_{\max} = 5 \times 10^{13} \text{ cm}^{-3}$ , and  $n_{\min} = 10^{13} \text{ cm}^{-3}$ . Here the radial coordinate  $r$  refers to the radius of each (essentially) circular flux surface with respect to its own center, *not* with respect to the magnetic axis. Thus, the density and temperature are constant on a flux surface, where the larger radii surfaces have the smallest densities and temperatures. The flux surfaces for this equilibrium exhibit just a small Shafranov shift ( $\Delta R < 15 \text{ cm}$ ), and, while not concentric, are essentially circular. Deuterium and tritium ions are in equal proportion. The pressure of  $\alpha$  particles is neglected. Given LH wave parameters  $\omega/2\pi = 4.5 \text{ GHz}$  and  $n_\phi = 2.5$ , we optimize over  $n_\theta$  and  $\theta$  for core penetration together with high current drive efficiency.

With these parameters, one-pass ray trajectories are then calculated using GENRAY [30], a geometrical optics code, which also calculates the linear Landau damping by electrons [31]. Assume the ray encounters a constant  $\alpha$ -particle gradient, arising from an  $\alpha$  particle birth distribution with decay length  $\lambda_\alpha$  in the region of wave propagation, and say constant otherwise, *i.e.*

$$\dot{N}_\alpha(r) = \begin{cases} \dot{N}_{\alpha 0} \exp(-r/\lambda_\alpha) & \text{if } r > r_{\text{closest}} \\ \dot{N}_{\alpha 0} & \text{otherwise} \end{cases}, \quad (9)$$

where  $r_{\text{closest}}$  is the distance of closest approach of the ray to the plasma center. The linear damping (or growth) rate due to  $\alpha$  particles can now be calculated along the ray trajectory, taking into account the linked diffusion in  $r - \epsilon_\perp$  space, according to Eq. (6), using the local radial coordinate, with Shafranov-shifted origin, in order to find the flux normal vector for each surface.

Consider, for example, a peak high-energy  $\alpha$  particle density of  $N_\alpha = (\dot{N}_{\alpha 0}/\nu) \log(3.5\text{MeV}/30\text{keV}) = 2.1 \times 10^{18} \text{ m}^{-3}$ , a radial decay length  $\lambda_\alpha = 2.20 \text{ cm}$ , and  $r_{\text{closest}} = 5.55 \text{ cm}$ . Ray trajectories that both produce large current drive efficiencies while penetrating near the magnetic axis can then be arranged by taking  $n_\theta = 1.5$  and  $\theta = 150^\circ$ . This ray features a sharp increase in the magnitude of  $k_\theta$  as it nears the center, strengthening  $\alpha$  channeling. This feature can be seen in the dramatic increase along the ray in the allowed radial decay length

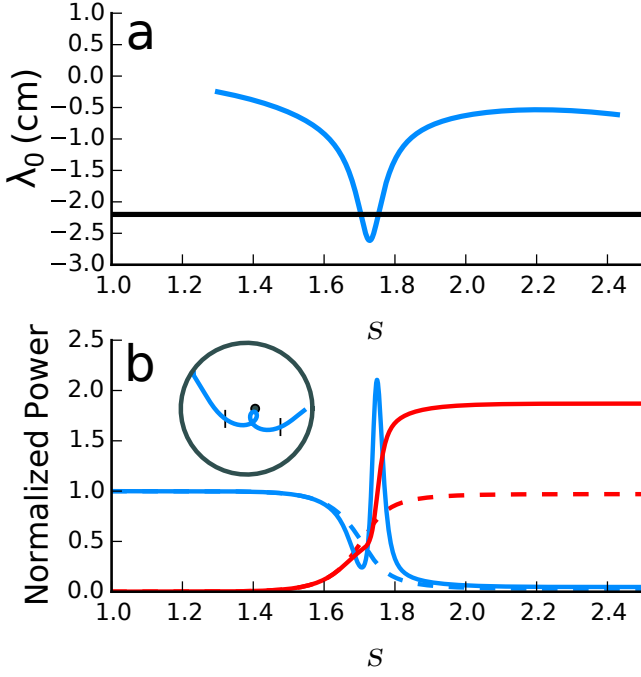


FIG. 3: The channeling effect in an ARC-like tokamak with  $n_\theta = 1.5$ . (a) Negative radial decay length in cm ( $\lambda_0$ ) of  $\alpha$  particles required for zero damping vs. poloidal length along ray. As the ray nears the plasma center ( $s \approx 1.73$  m), the maximum allowable decay length increases. Black line: imposed radial decay length of 2.2 cm. (b) Power remaining in ray (blue) and cumulative power delivered to electrons (red) along ray trajectory, both with (solid) and without (dashed) of  $\alpha$  particles present. Inset: poloidal trajectory; black lines indicate bounds of graphs. Color available online.

$\lambda_0$  (Fig. 3a). Also, near the center, the radial group velocity vanishes, so that this ray spends more time exactly where high-energy  $\alpha$  particles are abundant and with a steep gradient. Note that, while the ray is initially damped by electrons, it regains power from the  $\alpha$  channeling effect on the order of its initial power (Fig. 3b). As a result, the absorbed power by the electrons is almost twice the launched power in the ray. Moreover, as the ray propagates above the poloidal equator, its parallel phase velocity,  $\omega/k_\parallel$ , increases from  $0.38c$  at the plasma periphery to  $0.49c$  at  $r = 39$  cm, before decreasing to  $0.45c$  in its final approach to the plasma center, where the main absorption occurs nearest the magnetic axis. Thus, importantly, the main power is absorbed by electrons both on the tail of the velocity distribution (about 4.5 times the thermal velocity) and near the plasma center.

*Discussion:* Importantly, we can see that LH waves launched from the tokamak's high-field side, which are already predicted to be advantageous from an engineering standpoint [7, 8], can also avoid  $\alpha$ -particle damping or even experience amplification as they penetrate near the plasma center. When  $B_\phi > 0$  and  $k_\phi$  supports the plasma current, a ray trajectory that spends most of its

approach to the region of high  $\alpha$ -particle density below the poloidal equator is optimal for wave amplification. This generally occurs for wave launch from the inboard side. For concentric circular flux surfaces, we derived that the wave amplification conditions also necessarily result in a  $|k_\parallel|$  upshift in the region of strong damping for waves used to support the plasma current, and a  $|k_\parallel|$  downshift for those used to counteract the plasma current. For the general tokamak, this property will apply near the magnetic axis, where the geometry is effectively circular and where the key interactions take place. However, as we show in (Fig. 3b), a wave launched from the upper inboard side can experience an initial  $|k_\parallel|$  downshift, and then an upshift closer to the plasma center. Since a  $|k_\parallel|$  downshift results in decreased electron damping, such a strategy could result in stronger current drive near the plasma center.

For ARC-like parameters, we show how a population inversion can be achieved in the presence of a steep radial  $\alpha$ -particle birth gradient, with a decay length on the order of centimeters. For preliminary reactor experiments, fusion conditions are only marginally met in the plasma center, and not at all nearby, satisfying the requirement for a peaked energetic alpha particle distribution. However, in an advanced reactor, steep gradients are more difficult, and the alpha-distribution may be flattened along the diffusion paths when the waves are intense enough that a significant fraction of the alpha-particle energy is extracted [32]. In that case, the  $\alpha$  particles would not slow down significantly through collisions before being diffused to lower energy by the LH waves. To maintain the sharp spatial gradients, therefore, a second wave might be used in addition to the LH wave [33]. Note that the use here of a second wave is essentially different from other uses of a second wave to optimize the current drive efficiency [34–42], since rather than promoting absorption by higher velocity electrons, the second wave facilitates the absorption of energy to the LH wave from the  $\alpha$  particles. Both methods should lead to an effective increase in the efficiency.

The potential for  $\alpha$  channeling warrants experimental testing. However, the strict symmetries of the channeling effect and its coupling to the  $|k_\parallel|$  upshift present obstacles to testing these predictions directly. After all, the easiest differential test would be to leave all other parameters equal, but just to reverse  $k_\theta$ , with one sign resulting in damping and the other in amplification. However, as derived here, the strict coupling of  $k_\theta$  to the  $|k_\parallel|$  upshift renders this experiment impossible. In light of this, the best differential test might instead be to fix the wave conditions suitable for the channeling effect, both in the presence and absence of an energetic beam of ions. A similar differential test using neutral beams was performed successfully to test channeling effects predicted for the ion Bernstein wave [43].

*Conclusions:* The calculations here give a preferred

method of launch for LH waves supportive of the plasma current in the presence of  $\alpha$  particles, particularly for inside launch. The symmetries uncovered reveal the flexibilities and constraints on both optimizing and experimentally testing the effect. In an example case, the effective current drive efficiency is roughly doubled due to the  $\alpha$  channeling effect.

This work was performed under U.S. DOE contract DE-AC02-09CH11466. The authors are grateful to P. Bonoli for providing a GENRAY input file for an ARC-like equilibrium. One of us (IEO) thanks the support of the National Undergraduate Fellowship Program in Plasma Physics and Fusion Energy Sciences.

- 
- [1] N. J. Fisch, Physical Review Letters **41**, 873 (1978).
  - [2] N. J. Fisch, Rev. Mod. Phys. **59**, 175 (1987).
  - [3] K. L. Wong and M. Ono, Nuclear Fusion **24**, 615 (1984).
  - [4] N. J. Fisch and J. M. Rax, Nuclear Fusion **32**, 549 (1992).
  - [5] J. Wang, X. Zhang, L. Yu, and X. Zhao, Plasma Physics Reports **40**, 932 (2014).
  - [6] N. J. Fisch and J.-M. Rax, Phys. Rev. Lett. **69**, 612 (1992).
  - [7] Y. A. Podpaly, G. M. Olynyk, M. L. Garrett, P. T. Bonoli, and D. G. Whyte, Fusion Engineering and Design **87**, 215 (2012).
  - [8] B. Sorbom, J. Ball, T. Palmer, F. Mangiarotti, J. Sierchio, P. Bonoli, C. Kasten, D. Sutherland, H. Barnard, C. Haakonsen, et al., Fusion Engineering and Design (submitted) (2014).
  - [9] F. Imbeaux and Y. Peysson, Plasma Phys. Control. Fusion **47**, 2041 (2005).
  - [10] J. Decker, Y. Peysson, J. Hillairet, J. F. Artaud, V. Basiuk, A. Becoulet, A. Ekedahl, M. Goniche, G. T. Hoang, F. Imbeaux, et al., Nuclear Fusion **51**, 073025 (2011).
  - [11] Y. Peysson and J. Decker, Fusion Science and Technology **65**, 22 (2014).
  - [12] S. Ceccuzzi, E. Barbato, A. Cardinali, C. Castaldo, R. Cesario, M. Marinucci, F. Mirizzi, L. Panaccione, G. L. Ravera, F. Santini, et al., Fusion Science and Technology **64**, 748 (2013).
  - [13] W. Horton, M. Goniche, Y. Peysson, J. Decker, A. Ekedahl, and X. Litaudon, Physics of Plasmas **20**, 112508 (2013).
  - [14] J. Hillairet, D. Voyer, A. Ekedahl, M. Goniche, M. Kazda, O. Meneghini, D. Milanese, and M. Preynas, Nuclear Fusion **50**, 125010 (2010).
  - [15] E. Nilsson, J. Decker, Y. Peysson, J. F. Artaud, A. Ekedahl, J. Hillairet, T. Aniel, V. Basiuk, M. Goniche, F. Imbeaux, et al., Nuclear Fusion **53**, 083018 (2013).
  - [16] S. Xingjian, H. Yemin, and G. Zhe, Plasma Science & Technology **14**, 215 (2012).
  - [17] M. Schneider, L.-G. Eriksson, F. Imbeaux, and J. Artaud, Nuclear Fusion **49**, 125005 (2009).
  - [18] M. Spada, M. Bornatici, and F. Engelmann, Nuclear Fusion **31**, 447 (1991).
  - [19] E. Barbato and F. Santini, Nuclear Fusion **31**, 673 (1991).
  - [20] E. Barbato and A. Saveliev, Plasma physics and controlled fusion **46**, 1283 (2004).
  - [21] P. Bonoli and M. Porkolab, Nuclear fusion **27**, 1341 (1987).
  - [22] N. J. Fisch, Phys. Plasmas **2**, 2375 (1995).
  - [23] E. J. Valeo and N. J. Fisch, Phys. Rev. Lett. **73**, 3536 (1994).
  - [24] P. T. Bonoli and E. Ott, Physics of Fluids (1958-1988) **25**, 359 (1982).
  - [25] P. T. Bonoli and R. C. Englade, Physics of Fluids **29**, 2937 (1986).
  - [26] S. Bernabei et al., Phys. Rev. Lett. **49**, 1255 (1982).
  - [27] M. Porkolab, J. J. Schuss, B. Lloyd, Y. Takase, S. Texter, P. Bonoli, C. Fiore, R. Gandy, D. Gwinn, B. Lipschultz, et al., Physical Review Letters **53**, 450 (1984).
  - [28] C. F. F. Karney, N. J. Fisch, and F. C. Jobes, Physical Review A **32**, 2554 (1985).
  - [29] P. T. Bonoli, personal communication.
  - [30] A. Smirnov and R. Harvey, CompX Report CompX-2000-01 (2001).
  - [31] P. T. Bonoli, IEEE Transactions on Plasma science **12**, 95 (1984).
  - [32] N. J. Fisch and M. C. Herrmann, Nucl. Fusion **34**, 1541 (1994).
  - [33] N. J. Fisch and M. C. Herrmann, Nuclear Fusion **35**, 1753 (1995).
  - [34] I. Fidone, G. Giruzzi, G. Granata, and R. Meyer, Physics of Fluids **27**, 2468 (1984).
  - [35] I. Fidone, G. Giruzzi, V. Krivenski, E. Mazzucato, and L. Ziebell, Nuclear Fusion **27**, 579 (1987).
  - [36] R. Dumont and G. Giruzzi, Physics of Plasmas **11**, 3449 (2004).
  - [37] G. Giruzzi, J. Artaud, R. Dumont, F. Imbeaux, P. Bibet, G. Berger-By, F. Bouquey, J. Clary, C. Darbos, A. Ekedahl, et al., Physical review letters **93**, 255002 (2004).
  - [38] P. Rosa and L. Ziebell, Plasma Phys. Control. Fusion **44**, 2065 (2002).
  - [39] D. Farina and R. Pozzoli, Physics of Fluids B **1**, 815 (1989).
  - [40] Y. Dnestrovskij, D. Kostomarov, A. Lukyanitsa, V. Parail, and A. Smirnov, Nuclear Fusion **28**, 267 (1988).
  - [41] S. Y. Chen, B. B. Hong, Y. Liu, W. Lu, J. Huang, C. J. Tang, X. T. Ding, X. J. Zhang, and Y. J. Hu, Plasma Physics and Controlled Fusion **54**, 115002 (2012).
  - [42] J. Huang, S. Y. Chen, and C. J. Tang, Physics of Plasmas **21**, 012508 (2014).
  - [43] D. S. Clark and N. J. Fisch, Phys. Plasmas **7**, 2923 (2000).